Facile Synthesis of Highly Efficient Lepidine-Based Phosphorescent Iridium(III) Complexes for Yellow and White Organic Light-Emitting Diodes

Peng Tao, Wei-Ling Li, Jing Zhang, Song Guo, Qiang Zhao, Hua Wang,* Bin Wei, Shu-Juan Liu, Xin-Hui Zhou, Qi Yu, Bing-She Xu, and Wei Huang**

Highly efficient lepidine-based phosphorescent iridium(III) complexes with pentane-2,4-dione or triazolpyridine as ancillary ligands have been designed and prepared by a newly developed facile synthetic route. Fluorine atoms and trifluoromethyl groups have been introduced into the different positions of ligand, and their influence on the photophysical properties of complexes has been investigated in detail. All the triazolpyridine-based complexes display the blueshifted dual-peak emission compared to the pentane-2,4-dione-based ones with a broad single-peak emission. The complexes show emission with broad full width at half maximum (FWHM) over 100 nm, and the emissions are ranges from greenish–yellow to orange region with the absolute quantum efficiency (Φ_{PL}) of 0.21–0.92 in solution, i.e., Φ_{PL} = 0.92 (18), which is the highest value among the reported neutral yellow iridium(III) complexes. Furthermore, high-performance yellow and complementary-color-based white organic light-emitting diodes (OLEDs) have been fabricated. The FWHMs of the yellow, greenish–yellow OLEDs are in the range of 94–102 nm, which are among the highest values of the reported yellow or greenish–yellow-emitting devices without excimer emission. The maximum external quantum efficiency of monochrome OLEDs can reach 24.1%, which is also the highest value among the reported yellow or greenish–yellow devices. The color rendering indexes of blue and complementary yellow-based white OLED is as high as 78.

1. Introduction

Considerable progress has been made in the design and synthesis of phosphorescent transition-metal complexes suitable for organic light-emitting diodes (OLEDs) that are regarded as potential replacements in future display and solid-state lighting techniques.[1–15] The phosphorescent transition-metal complexes harness both singlet and triplet excitons to improve device efficiency greatly compared with electrofluorescent emitters.[16–20] To meet the target of full-color flat-panel displays and low-cost lighting sources, recent efforts have been devoted to the color tuning of these complexes.[21–27] Among all kinds of transition-metal complexes, the cyclometalated iridium(III) complexes are considered as the most attractive candidates for electroluminescent devices owing to their stable chemical structure, high luminescent efficiency, and tunable emission wavelength over the whole visible region.[28–32]

The greenish–yellow or yellow emission is one crucial chromaticity component to high-performance white OLEDs (WOLEDs).[33–35] Usually, the WOLEDs are made up of three primary colors (RGB),[16,19,36–39] so there is a great gap (up to 100 nm) in the white-light spectrum because the wavelengths of typical green and red emitters are 520 and 620 nm, respectively, leading to the uncontinuity of the spectrum of WOLEDs. In other words, the emission in the range from 520 to 620 nm is missing, which greatly affects

P. Tao, Prof. H. Wang, Prof. B.-S. Xu
Research Center of Advanced Materials Science and Technology and MOE Key Laboratory of Interface Science and Engineering in Advanced Materials
Taiyuan University of Technology
Taiyuan 030024, P. R. China
E-mail: wanghua001@tyut.edu.cn

P. Tao, S. Guo, Prof. Q. Zhao, Prof. S.-J. Liu, Prof. X.-H. Zhou, Q. Yu
Key Laboratory for Organic Electronics and Information Displays and Institute of Advanced Materials (IAM)
Jiangsu National Synergetic Innovation Center for Advanced Materials (SICAM)
Nanjing University of Posts and Telecommunications (NUPT)
Nanjing 210023, P. R. China
E-mail: iamqzhao@njupt.edu.cn

W.-L. Li, J. Zhang, Prof. B. Wei
MOE Key Laboratory of Advanced Display and System Applications
Shanghai University
Shanghai 200072, P. R. China

Prof. W. Huang
Key Laboratory of Flexible Electronics (KLOFE) and Institute of Advanced Materials (IAM)
Jiangsu National Synergetic Innovation Center for Advanced Materials (SICAM)
Nanjing Tech University (NanjingTech)
Nanjing 211816, P. R. China
E-mail: wei-huang@njtech.edu.cn

DOI: 10.1002/adfm.201503826

© 2015 WILEY-VCH Verlag GmbH & Co. KGaA, Weinheim

the color rendering indexes (CRI) of WOLEDs. To solve this problem, one way is to incorporate yellow emitter into RGB-based WOLEDs,[33,34] and the other is to directly replace the green emitter or replace both green and red emitters by a greenish–yellow emitter with broad full width at half maximum (FWHM).[40–42] For the first approach, much more complicated device structures are needed, although the incorporation of yellow emitter into RGB-based WOLEDs can be effective to increase the CRI of WOLEDs. In contrast, combination of blue and complementary yellow emissions is more attractive. So the phosphors exhibiting greenish–yellow and yellow emission, especially, with broad FWHM become very significant for high-quality device fabrication. Recently, some efforts have been devoted to broaden the FWHM of yellow or greenish–yellow-emitting OLEDs. Lee et al.[35] reported yellow-emitting OLEDs incorporating 2-(2-naphthyl)pyridine-based iridium(III) complex with much broader FWHM up to 87 nm. Li et al.[43] and Laskar et al.[44] have demonstrated yellow phosphorescent OLEDs with FWHMs over 100 nm by utilizing excimer emission induced by platinum(II) complexes with low efficiencies of 6.6 and 2.4 lm W^{-1}. However, the electroluminescence (EL) spectra and the corresponding 1931 Commission Internationale de L'Eclairage (CIE) coordinates based on excimer emission are greatly influenced by the dopant concentration. Li et al.[45] reported 2-aryl-benzothiazole-based iridium(III) complexes exhibiting yellow emission with the solution quantum efficiency (Φ_{PL}) of 0.34–0.42, and the device with external quantum efficiency (EQE) of 23.0% based on yellow emitter was achieved. Hou et al.[46] reported bis(pyridylphenyl) iridium(III) complexes bearing ancillary guanidinate ligands with emission wavelength (λ_{max}) of 528–560 nm and Φ_{PL} of 0.16–0.37. Jou et al.[47] reported 5-methyl-7-fluoro-5*H*-benzo[c][1,5]naphthyridin-6-one-based iridium(III) complex emitting at 545 nm with Φ_{PL} up to 0.71, and the EQE of yellow device with FWHM of 80 nm is up to 22.6%. Dumur et al.[48] reported an iridium(III) complex containing 7,8-benzoquinoline as the cyclometalated ligand emitting at 551 nm, and the FWHM of the device is 75 nm. Chang et al.[33] reported a greenish–yellow emitter [bis(2-methyldibenzo[*f*,*h*]quinoxaline) tetrakis(1-pyrazolyl)-borate iridium(III)] with Φ_{PL} up to 0.74. Using this greenish–yellow emitter, the device with EQE of 21.5% can be obtained. However, the relatively narrow FWHM (63 nm) of the device is achieved. Cao et al.[49] reported the blue- and red-based WOLEDs with low CRI of 52 due to the bad match of blue and red emission. They also fabricated a blue-orange codoped WOLED.[50] The resulting moderate color quality with a CRI falling in the narrow range of 52–55 was not impressive, which can be attributed to the very narrow FWHM (50 nm) of orange emitter used. Recently, Xie et al.[18] reported a blue-orange complementary-color-based phosphorescent WOLED exhibiting the relatively low CRI of 65, which is caused by the narrow FWHM (63 nm) of orange emitter used. Very recently, Ye et al.[51] reported the binary blue and complementary orange color WOLEDs with a high CRI of 71.

Considering that the performance of greenish–yellow or yellow emitters is significantly behind those emitting in the three primary colors, it is urgent to design and synthesize these phosphorescent emitters with high quantum efficiency and broad width at half maximum, which are driven by the solid-state lighting industry.[33,34,40–48] 2-Phenylquinoline (HPQ) is an excellent cyclometalated ligand, and red or deep red-emitting phosphors derived from HPQ have been reported.[52–55] However, the greenish–yellow or yellow emitters based on HPQ derivatives are quite rare.[56] From the perspective of molecular design, the photophysical properties of the phosphorescent complexes can be tuned by choosing different types of cyclometalated or ancillary ligands, or introducing special functional groups to the ligands.[57] For instance, using fluorine (F) atom or trifluoromethyl (CF_3) group to replace hydrogen in the cyclometalated ligand could alter the energy levels of emitters, i.e., the highest occupied molecular orbital (HOMO) and the lowest unoccupied molecular orbital (LUMO), which may in turn allow the tuning of emission colors.[58] Fluorination can also be used to markedly reduce concentration quenching of luminescence and meanwhile increase volatility to favor vapor deposition.[59] In most cases, fluorination can enhance electron mobility, resulting in a more balanced carrier injection and hence a higher device efficiency.[60] In previous studies, triazolpyridine,[61,62] which is a well-known ancillary ligand for its remarkable blueshifting capability than that of *β*-diketonates by reducing the HOMO level of the iridium(III) complex, is usually introduced into iridium(III) complexes to achieve deep blue emission. Thus, the triazolpyridine ligand could have a potential application in design of yellow-emitting iridium(III) complex. For the commonly used synthetic route of *β*-diketonate-based and triazolpyridine-based neutral iridium(III) complexes, there are two steps: (i) the cyclometalated iridium(III)-chloro-bridged dimers of a general formula $(C^{\wedge}N)_2Ir(\mu\text{-}Cl)_2Ir(C^{\wedge}N)_2$ were synthesized according to the Nonoyama route by refluxing $IrCl_3 \cdot 3H_2O$ with 2.0–2.5 equiv. of cyclometalated ligand in a 3:1 (V:V) mixture of 2-ethoxyethanol and water;[63] (ii) the chloro-bridged dimers together with 2.5 equiv. of ancillary ligands and 10 equiv. of anhydrous Na_2CO_3 were refluxed at 110 °C under an inert atmosphere in 2-ethoxyethanol for 24 h. Thus, the high boiling 2-ethoxyethanol and harsh reaction condition are required, especially in the second step. What's more, intermediate complexes have a potential risk of oxidation process or thermal decomposition, especially for complex containing sensitive functional groups at such a high-temperature reaction, leading to hard purification and low yields. Hence, the convenient synthetic methods are needed for the preparation of phosphorescent complexes.

Herein, we developed a more facile method to prepare both *β*-diketonate-based and triazolpyridine-based neutral iridium(III) complexes. That is, the corresponding chloro-bridged dimers together with 2.2 equiv of *β*-diketonate or triazolpyridine were stirred under very mild condition with dichloromethane as solvent and anhydrous potassium carbonate as deacid reagent at room temperature (≈25 °C). The complexes obtained by this method are easy to be purified with high yields. By modifying the phenyl ring of HPQ ligand with one or more F atoms and (or) CF_3 group or choosing suitable ancillary ligands (*β*-diketonate or triazolpyridine), as shown in Scheme 2, we realized the effective color tuning of iridium(III) phosphors in the range of greenish–yellow, yellow, and orange-yellow emission (emission wavelength from 545 to 597 nm) with markedly improved phosphorescent quantum efficiency (up to 0.92, the highest value among the reported neutral yellow iridium(III)

© 2015 WILEY-VCH Verlag GmbH & Co. KGaA, Weinheim

complexes) and the broad emission bands (FWHM up to 103 nm). In addition, we also introduced a methyl group into 4-position of quinoline ring to increase solubility in organic solvents and to suppress triplet-triplet annihilation of iridium(III) complexes.[64] Based on the newly synthesized complexes, highly efficient monochrome yellow, greenish–yellow and complementary-color-based white OLED have been fabricated. The FWHMs of the fabricated OLEDs are in the range of 94–102 nm, which are among the highest values of the reported yellow or greenish–yellow-emitting devices without excimer emission. The maximum EQE of monochrome devices based on complex **9**, **13**, **15**, **17**, and **18** are in the range of 20.8%–24.1%, respectively. Especially, the maximum EQE of device based on **9** is up to 24.1%, which is the highest value among the reported yellow or greenish–yellow OLEDs. And the CRI of blue and complementary yellow-based WOLED is as high as 78.

2. Results and Discussion

2.1. Synthesis and Characterization

The cyclometalated H*C^N* ligands (abbreviated HMePQ, HMePQ-4F, HMePQ-24F, HMePQ-234F, HMePQ-35F, HMePQ-345F, HMePQ-2345F, HMePQ-3CF_3, and HMePQ-3CF_3-4F), as shown in **Scheme 1**, were synthesized by highly efficient Suzuki coupling reaction between the corresponding fluorine-containing arylboronic acid and 2-chloro-4-methylquinoline. The key intermediate compound 2-chloro-4-methylquinoline was synthesized by three-step reactions in overall yields of 74%. The isolated yields of the new cyclometalated ligands are ≈81%–93% (Scheme S1, Supporting Information). The F atom(s) and (or) CF_3 group were successfully introduced into the H*C^N* ligands. The new cyclometalated H*C^N* ligands were fully characterized by nuclear magnetic resonance (^{1}H NMR, ^{13}C{^{1}H} NMR and ^{19}F{^{1}H} NMR).

The chemical structures of the Ir(*C^N*)$_2$(acac) and Ir(*C^N*)$_2$(4FPZ) complexes are shown in **Scheme 2**. The newly synthesized iridium(III) complexes can be divided into two classes according to the different ancillary ligands of pentane-2,4-dione (Hacac) or 2-(3-(4-fluorophenyl)-1*H*-1,2,4-triazol-5-yl)-pyridine (H4FPZ). The change of ancillary ligands is intended to further tune the phosphorescent energy. What's more, the F atom(s) and (or) CF_3 group bonded to *C^N* ligands of the iridium(III) complexes could not only finely tune the energy gap but also greatly affect the quantum efficiency of complexes.

The synthetic procedures of iridium(III) complexes are shown in Scheme S2 (Supporting Information). Cyclometalated iridium(III) μ-chlorobridged dimers of a general formula (*C^N*)$_2$Ir(μ-Cl)$_2$Ir(*C^N*)$_2$ were synthesized according to the reported Nonoyama route.[63] Notably, different from commonly used synthetic method of neutral iridium(III) complexes,[64,65] a more facile way to prepare both *β*-diketonate-based and triazolpyridine-based iridium(III) complexes was presented here for the first time, that is, the corresponding chlorobridged dimers together with 2.2 equiv. of Hacac or H4FPZ were stirred under very mild condition with dichloromethane as solvent and anhydrous potassium carbonate as deacid reagent at room temperature (≈25 °C), This mild condition leads to the easy treatment and purification of the target iridium(III) complexes in high yields of ≈75%–92%, which is very important for the future large-scale preparation of phosphorescent complexes.

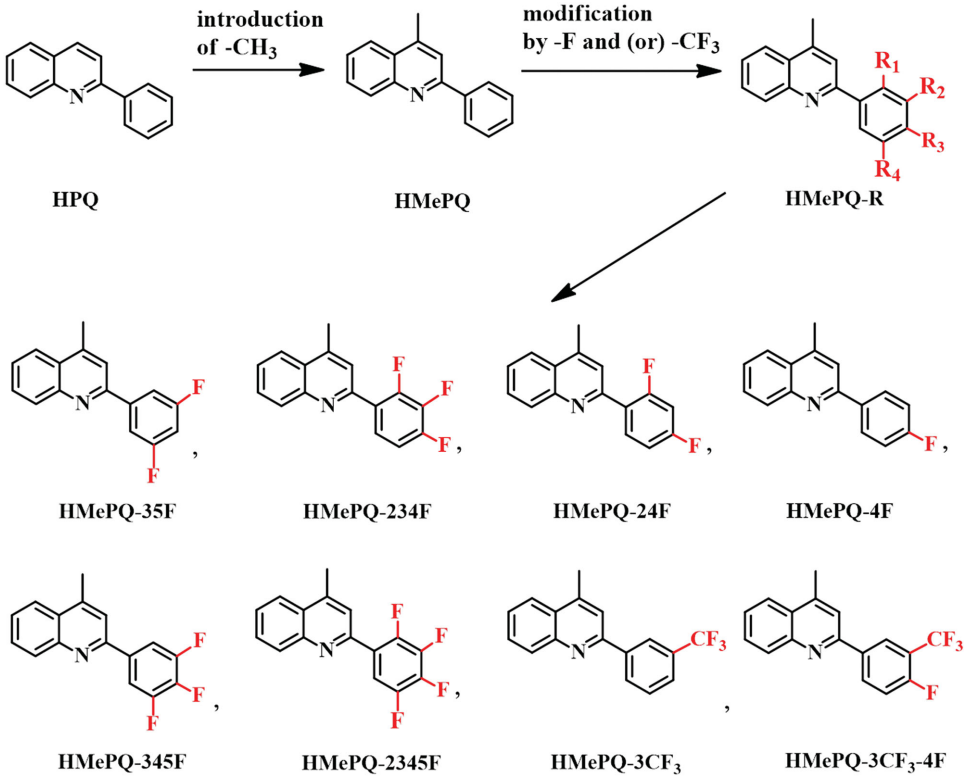

Scheme 1. Illustration of the modification of 2-phenylquinoline by fluorine atoms and (or) a trifluoromethyl (CF_3) group.

© 2015 WILEY-VCH Verlag GmbH & Co. KGaA, Weinheim

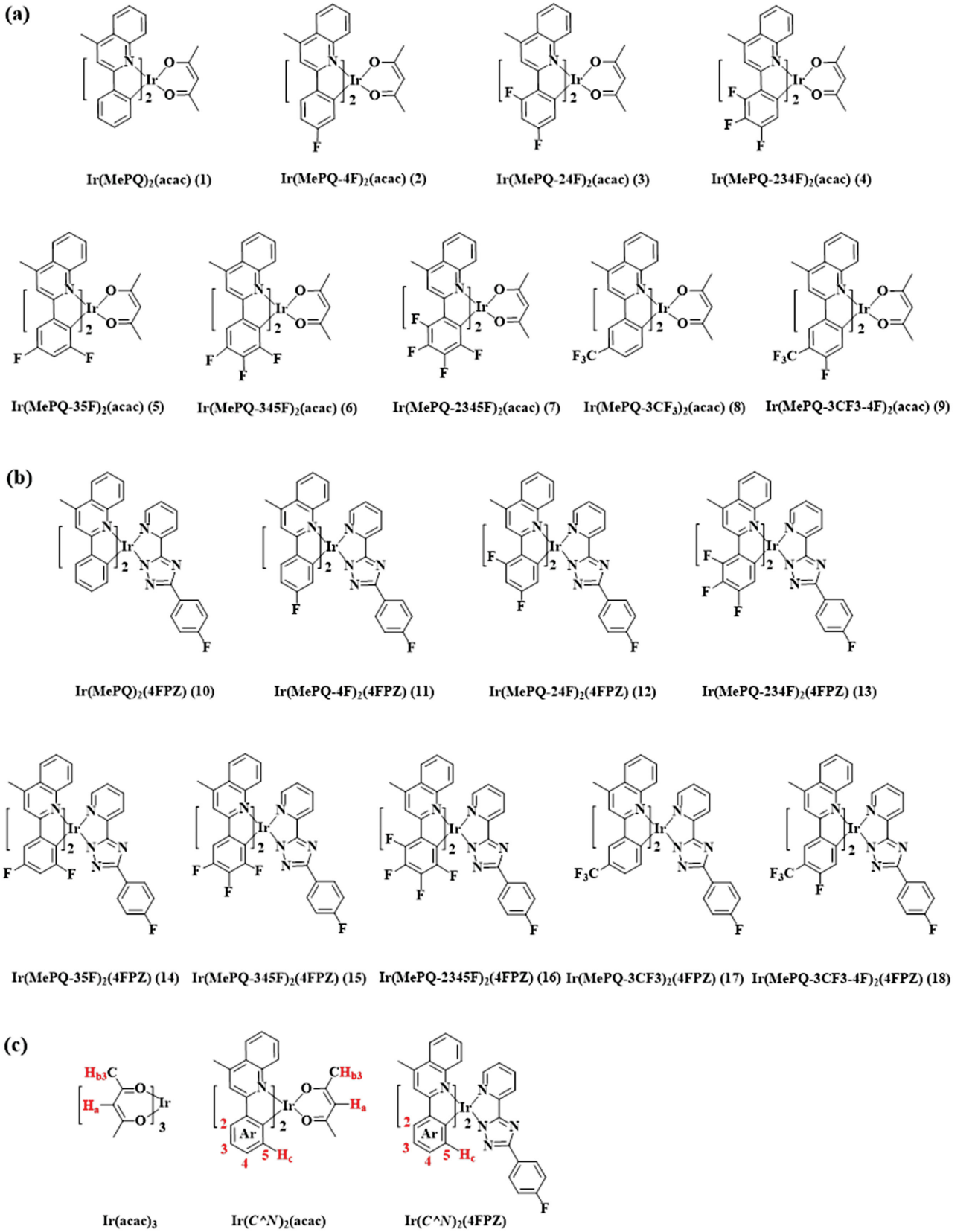

Scheme 2. The chemical structures of the complexes a) Ir(C^N)$_2$(acac), b) Ir(C^N)$_2$(4FPZ), c) and the abbreviations of selected protons, labels of position in iridium(III) complexes.

© 2015 WILEY-VCH Verlag GmbH & Co. KGaA, Weinheim

Using commonly synthetic method under the condition of 2-ethoxyethanol and anhydrous sodium carbonate at 100 °C, unexpectedly, gave low yields of products. Especially for Ir(MePQ-234F)$_2$(4FPZ) (**13**), no products could be obtained from its chlorobridged dimer and H4FPZ ligand under that condition, and the unexpected complex **19** with one F atom replaced by 2-ethoxyethanol in each cyclometalated ligand was isolated and identified (Scheme S3 and Figure S1, Supporting Information), which is probably the result of easily occurring substitution process of the fluorine by 2-ethoxyethanol under that condition. So the commonly used synthetic method is not suitable for the preparation of multifluorine-containing neutral iridium(III) complexes. All iridium(III) complexes have been fully characterized by ^{1}H NMR, ^{13}C{^{1}H} NMR and ^{19}F{^{1}H} NMR (^{13}C{^{1}H} NMR was not recorded for all Ir(*C^N*)$_2$(4FPZ) because of their poor solubility) and matrix-assisted laser desorption ionization time-of-flight mass spectrometry (MALDI-TOF-MS). The structures of complexes **1**, **2**, **4**, **6**, **7**, **9**, and **15** were further confirmed by single-crystal X-ray diffraction.

The NMR spectra (shown in the Supporting Information) of all iridium(III) complexes show the clearly well-resolved resonance signals, indicating that the complexes have a high purity suitable for device fabrication. The two cyclometalated ligands in the acac-based complexes, i.e., MePQ-4F, are equivalent to each other owing to the symmetry of ancillary ligand acac as evidenced by 11 resonances in the ^{1}H NMR spectrum (Figure S2a, Supporting Information) and 19 resonances (not considering the extra splitting of ^{13}C affected by ^{19}F nucleus) in the ^{13}C{^{1}H} NMR spectrum (Figure S2b, Supporting Information) of Ir(MePQ-4F)$_2$(acac), supporting that the acac-based complexes possess a configuration with C_2 symmetry. In contrast, this symmetry is lost in complex Ir(*C^N*)$_2$(4FPZ). This molecular symmetry of complexes is also consistent with ^{19}F resonance signals in ^{19}F{^{1}H} NMR spectrum. Protons adjacent to the C—Ir bonds (H_c protons in Ir(*C^N*)$_2$(acac) and Ir(*C^N*)$_2$(4FPZ) in Scheme 2c) are susceptible to shielding because of ring current perturbation from an adjacent ligand,[66] thereby suggesting high-field assignments of these protons (5.97–6.51 ppm for Ir(*C^N*)$_2$(acac) (Table S1, Supporting Information) and 5.92–6.75 ppm for Ir(*C^N*)$_2$(4FPZ) (Table S2, Supporting Information)). Moreover, the acetylacetonate CH_a protons in Ir(*C^N*)$_2$(acac) appear in the region of 4.53–4.69 ppm as a sharp singlet (Table S1, Supporting Information). For the control complex Ir(acac)$_3$, this signal appears at 5.49 ppm (Table S1, Supporting Information). The acetylacetonate CH_a protons in Ir(*C^N*)$_2$(acac) are more shielded due to the ring current perturbation from two cyclometalated ligands.[55] The above-mentioned shielding effect is also manifested on the chemical shift of the acetylacetonate CH_{b3} protons. In Ir(acac)$_3$ complex they are observed at 2.01 ppm (Table S1, Supporting Information), while in the present acac-based complexes they resonate from 1.46 to 1.53 ppm (Table S1, Supporting Information).

In addition, we evaluated the chemical stability of the complex **13** and **9** (as examples) by thermogravimetric analysis, as shown in Figure S3 (Supporting Information). From the thermogravimetric curves, the decomposition temperatures of 5% weight loss of both complexes exceed 300 °C, indicating that the two complexes exhibit sufficient thermal stability for application in OLEDs. Moreover, the decomposition temperature of **13** is higher than that of **9**, which is probably owing to higher molecular weight.

2.2. X-ray Structure Determination

The single crystals of acac-based irdium(III) complexes **1**, **2**, **4**, **6**, **7**, and **9** suitable for X-ray diffraction analysis were grown from dichloromethane solutions, while the single crystal of 4FPZ-based complex **15** was obtained from dimethyl sulfoxide solutions. The crystallographic refinement parameters of complexes **1**, **2**, **4**, **6**, **7**, **9**, and **15** are summarized in Tables S3–S5 (Supporting Information), respectively. ORTEP plots of these complexes are displayed in **Figure 1**. The iridium center adopts a distorted octahedral coordination geometry with *cis*-metalated carbons and *trans*-phenylquinoline nitrogen atoms, the same as previously observed in other analogous complexes.[48] From the ORTEP plots of the isomers **4** and **6**, it is shown clearly that the three F substituents located in the 2,3,4-positions of phenyl ring in complex **4**, whereas in the 3,4,5-positions in complex **6**, which causes different electronic effects and then different photophysical properties. The four F atoms in the phenyl ring of each cyclometalated H*C^N* ligand of complex **7** are undoubtedly confirmed by its single-crystal structure, indicating that the four F atoms of cyclometalated H*C^N* ligand can be maintained in the synthesis of the corresponding μ-chlorobridged dimers. In the crystal of **9**, the two bulky CF_3 substituents are in the *para* position of iridium atom rather than in the *ortho* position, which is the result of van der Waals repulsion between the bulky CF_3 group and the π plane of another ligand. For 4FPZ-based complex **15**, the center Ir atom bonds to nitrogen atom in the 1-position of 1,2,4-triazol ring due to the steric hindrance effect of the bulky 4-fluorophenyl moiety, which is also revealed by its ORTEP plot. The F atoms and (or) CF_3 group also have great effects on the crystal packing of the complex. There are three kinds of π–π interactions observed in these complexes (Figures S4–S10, Supporting Information), that is, π–π interactions between lepidine ring and lepidine ring, lepidine ring and (F and (or) CF_3 modified) phenyl ring, (F and (or) CF_3 modified) phenyl ring and (F and (or) CF_3 modified) phenyl ring. In the fluorine-free complex **1**, there exist two kinds of weak intermolecular π–π interaction. One is between the lepdine units (the distance is 3.70 Å), and the other is between the lepdine unit and phenyl ring (the distance is 3.60 Å) from two different molecules. Note that the two CH_3 groups located in the 4-position of quinoline ring of these complexes are far away from each other, which effectively increase the distance among iridium(III) complexes and thus suppress triplet–triplet annihilation of iridium(III) complexes.

2.3. Photophysical Properties

The absorption and emission spectra of all complexes were measured at room temperature in dichloromethane (**Figure 2**). All acac-based fluorine-containing complexes feature the intense absorption bands in the region of 250–360 nm, assigned to $^1\pi\rightarrow\pi^*$ transition of ligand (^{1}LC), and show ≈5 nm blueshift

© 2015 WILEY-VCH Verlag GmbH & Co. KGaA, Weinheim

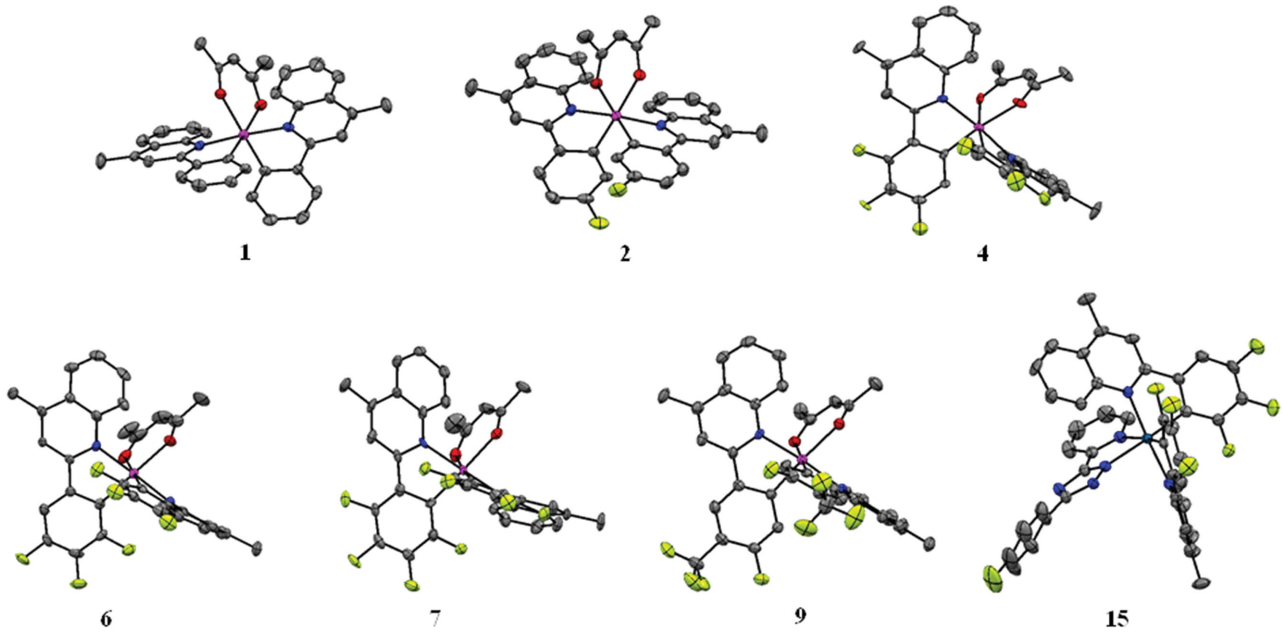

Figure 1. ORTEP diagrams of the complexes **1**, **2**, **4**, **6**, **7**, **9**, and **15** with thermal ellipsoids drawn at the 30% probability level and H atoms, solvent molecules removed for clarity.

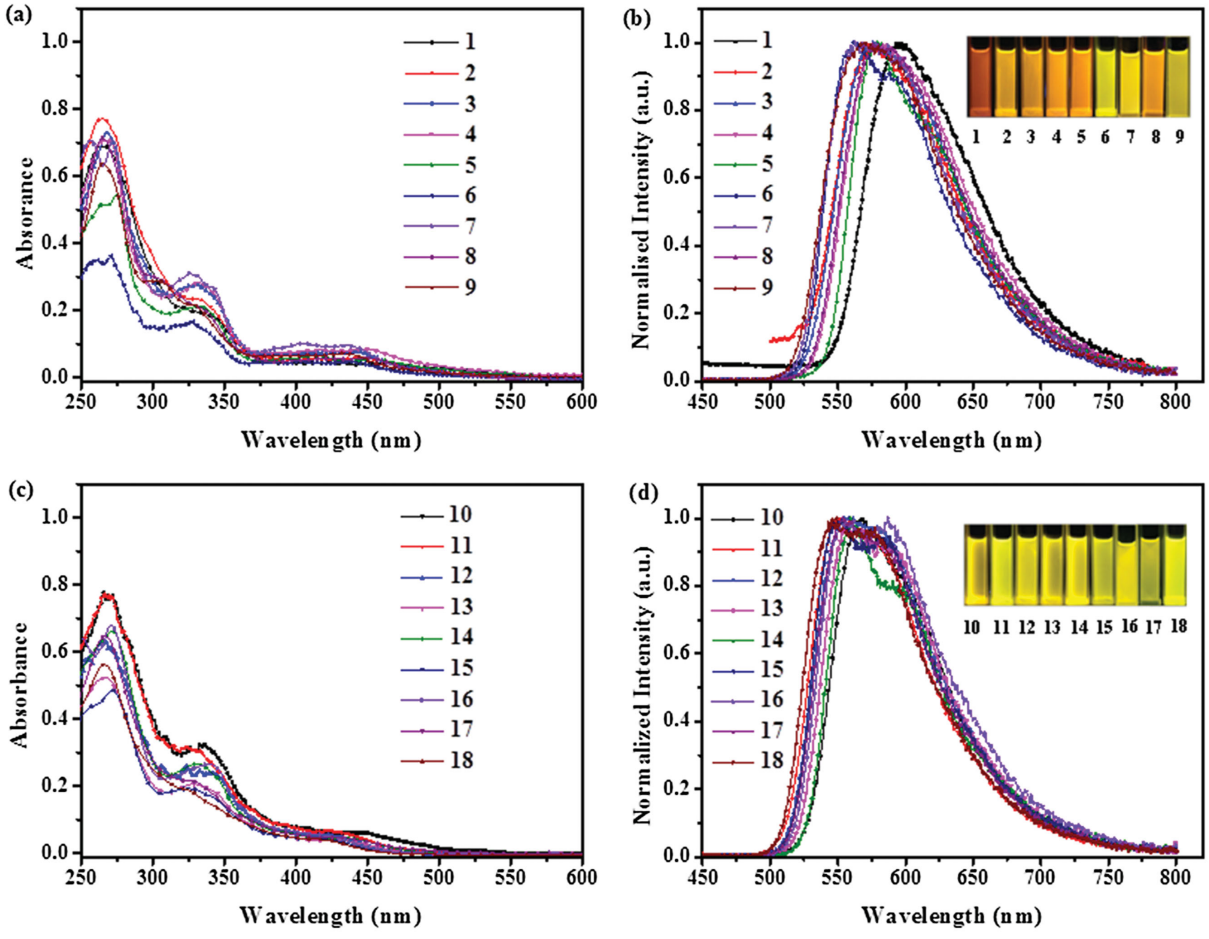

Figure 2. a) UV–vis absorption and b) photoluminescence spectra of **1–9** in CH_2Cl_2; c) UV–vis absorption and d) photoluminescence spectra of **10–18** in CH_2Cl_2. Inset: Luminescence photographs of **1–18** in CH_2Cl_2.

© 2015 WILEY-VCH Verlag GmbH & Co. KGaA, Weinheim

related to the fluorine-free complex Ir(MePQ)$_2$(acac) (**1**) due to the electron-withdrawing nature of F atoms and (or) CF_3 group in the phenyl ring of cyclometalated ligands. The weak bands in the range of 360–550 nm are likely assigned to the singlet and triplet metal-to-ligand charge-transfer transitions (^{1}MLCT and ^{3}MLCT) (Figure 2a). The similar absorption properties were observed for all 4FPZ-based complexes (Figure 2c). It is notable that MLCT bands of 4FPZ-based complex exhibit the obvious blueshift related to those of the corresponding acac-based complex. This indicates that the ancillary ligand H4FPZ exhibits the strong ability to induce the blueshift of spectral properties of phenyl quinoline-based iridium(III) complexes.

The introduction of F atoms and (or) CF_3 group into Ir($C^\wedge N$)$_2$(acac) or Ir($C^\wedge N$)$_2$(4FPZ) has great effect on the emission spectra. First, both the acac-based and 4FPZ-based complexes show obvious blueshift emission related to the corresponding fluorine-free complexes, indicating the electron-withdrawing nature of F atoms and (or) CF_3 group in the phenyl ring of cyclometalated ligands. Correspondingly, the emission color is changed from red for the fluorine-free complex **1** to orange–yellow and yellow for Ir($C^\wedge N$)$_2$(acac), and from yellow for the fluorine-free complex **10** to greenish–yellow for Ir($C^\wedge N$)$_2$(4FPZ). The acac-based complexes exhibit broad and featureless emission peaks in the range of 560–597 nm with the absolute quantum yields of 0.21–0.80 in CH_2Cl_2 and the emission lifetime (τ) of 0.33–7.45 μs (Figure 2b and **Table 1**). In contrast, the 4FPZ-based complexes show dual emission peaks, and the emissions are in the range of 545–567 nm with the absolute quantum yields of 0.36–0.92 and the lifetime of 1.03–6.77 μs in CH_2Cl_2 (Figure 2d and Table 1). More notably, both Ir($C^\wedge N$)$_2$(acac) and Ir($C^\wedge N$)$_2$(4FPZ) exhibit very broad FWHMs in the range of 87–103 nm (Table 1), which is of great importance in enhancing the CRI of white devices, especially for the blue and complementary yellow-based WOLEDs with the simple device structure. Moreover, F atoms and (or) CF_3-substitution remarkably improve phosphorescence efficiency owing to the rigidity of carbon–fluorine bond than that of carbon–hydrogen bond, for example, Φ_{PL} = 0.92 (**18**) versus 0.35 (control complex **10**), the highest value among the reported neutral yellow iridium(III) complexes.[47] These results suggest that the fluorine substituents on the cyclometalated ligands play a significant role in controlling the excited-state properties. Compared to the pentane-2,4-dione ligand of acac-based complex, the auxiliary ligand triazolpyridine of 4FPZ-based complex has less electron-donating ability to the Ir center due to the more delocalization effect of π electrons within the conjugated π system. This relatively weak electron-donating ability to the Ir center effectively stabilized the HOMO orbital of the 4FPZ-based complex, thus, the HOMO energy level was decreased and then the energy gap of lepidine-based iridium(III) complex was enlarged. Hence the blueshift of emission spectra was observed. This is well consistent with the fact that the more positive oxidations for 4FPZ-based complexes are observed than those for acac-based complexes, which will be further discussed in the following section of electrochemical properties.

The low-temperature phosphorescence spectra of the complexes were measured in a glass 2-methyltetrahydrofuran (2-MeTHF) matrix at 77 K (Figure S11, Supporting

Table 1. Absorption, luminescence, and electrochemical data for iridium(III) complexes.

Complex	Absorption[a] λ_{abs} [nm] (lg ε)	Emission[b]				E_{onset}^{oxc} [eV]	E_g[d] [eV]	HOMO/LUMO[d] [eV]
		λ_{em} [nm]	FWHM [nm]	τ [μs]	Φ_{PL}			
1	265(4.83), 341(4.26), 463(3.59), 510(3.36), 549(2.94)	597	93	0.33	0.21	0.53	2.08	–5.33/–3.25
2	263(4.89), 334(4.37), 444(3.76), 497(3.33), 531(2.96)	574	98	0.46	0.24	0.65	2.16	–5.45/–3.29
3	269(4.86), 330(4.45), 407(3.85), 443(3.89), 537(2.63)	577	100	0.77	0.52	0.79	2.15	–5.59/–3.44
4	269(4.64), 330(4.24), 446(3.71), 509(3.15), 549(2.53)	584	101	0.88	0.60	0.80	2.12	–5.60/–3.48
5	272(4.51), 329(4.14), 454(3.54), 502(3.12), 548(2.83)	579	90	0.81	0.62	0.69	2.14	–5.49/–3.35
6	271(4.56), 328(4.22), 442(3.68), 494(3.07), 539(2.70)	564	95	0.71	0.75	0.81	2.20	–5.61/–3.41
7	272(4.75),325(4.30), 403(3.73), 438(3.73), 523(2.68)	564	103	7.45	0.64	0.98	2.20	–5.78/–3.58
8	265(4.85), 336(4.31), 450(3.78), 499(3.30), 533(2.56)	578	98	0.69	0.70	0.77	2.16	–5.57/–3.41
9	268(4.71), 324(4.27), 435(3.76), 495(3.07), 534(2.70)	560	103	1.58	0.80	0.89	2.21	–5.69/–3.48
10	269(4.90), 336(4.53), 398(3.92), 443(3.81), 504(3.33)	567	88	1.03	0.35	0.69	2.19	–5.49/–3.30
11	267(4.91), 324(4.53), 424(3.88), 462(3.43), 498(2.92)	552	96	1.05	0.51	0.84	2.25	–5.64/–3.39
12	265(4.82), 324(4.43), 424(3.79), 445(3.39), 490(1.97)	559	101	1.73	0.63	0.97	2.22	–5.77/–3.55
13	267(4.72), 328(4.32), 384(3.75), 432(3.62), 493(1.59)	559	92	1.88	0.91	1.00	2.22	–5.80/–3.58
14	271(4.82), 330(4.42), 393(3.80), 434(3.67), 504(1.59)	560	87	1.57	0.89	0.89	2.21	–5.69/–3.48
15	272(4.68), 324(4.28), 392(3.69), 422(3.62), 485(2.54)	550	98	1.62	0.87	1.01	2.25	–5.81/–3.56
16	271(4.74),340(4.31), 396(3.71), 420(3.70), 457(2.60)	554	103	6.77	0.83	1.16	2.24	–5.96/–3.72
17	267(4.81), 330(4.33), 386(3.83), 435(3.68), 483(3.18)	554	96	1.44	0.88	0.96	2.28	–5.76/–3.48
18	266(4.75), 324(4.28), 388(3.74), 422(3.62), 468(2.55)	545	100	1.69	0.92	1.05	2.28	–5.85/–3.57

[a]At a concentration of 1.0 × 10^{-5} mol L^{-1} in CH_2Cl_2; [b]At a concentration of 1.0 × 10^{-5} mol L^{-1} in degassed CH_2Cl_2, λ_{ex} = 365 nm; [c]In CH_2Cl_2; [d]HOMO (eV) = –e(E_{onset}^{ox} + 4.8), E_g = 1240/λ, LUMO (eV) = E_g + HOMO.

© 2015 WILEY-VCH Verlag GmbH & Co. KGaA, Weinheim

Information). All of the complexes show obvious blueshift of the emission maxima with fine structures of vibronic bands (Table S6, Supporting Information), which is different from the broad and featureless emission spectra at room temperature discussed above. And the triplet energy (T_1) levels were estimated from the highest-energy vibronic subband of the phosphorescence spectra. The T_1 are summarized in Table S6 (Supporting Information). The Ir($C^{\wedge}N$)$_2$(4FPZ) exhibit higher T_1 than the corresponding acac-based complexes, for example, T_1 = 2.27 eV (**13**) versus 2.21 eV (**4**), which is consistent with the fact that the triazolpyridine-based complexes display the blueshifted emission compared to the pentane-2,4-dione-based ones at room temperature.

2.4. Electrochemical Properties

The electrochemical properties of all complexes were examined by cyclic voltammetry in CH_2Cl_2 solution (Figure S12, Supporting Information). Both acac-based and 4FPZ-based complexes have reversible oxidation waves with potentials in the range of 0.53–1.16 V (Table 1). We attribute this positive oxidation potential to the Ir centered oxidation. The oxidation potentials of acac-based complexes containing fluorine atoms show a positive shift of ≈0.45 V in comparison to the corresponding Ir(MePQ)$_2$(acac) (**1**), demonstrating that more electron-withdrawing nature of the ligands may result in the variation in the electronic properties at the metal center. The values of oxidation potentials of acac-based complexes follow the order of **9** > **8** > **6** > **4** > **3** > **7** > **5** > **2** > **1**, and those of 4FPZ-based complexes follow the order of **18** = **17** > **15** > **13** > **12** > **16** > **14** > **11** > **10**, indicating that the electron-withdrawing ability of the fluorine was not only affected by the number of the fluorines or trifluoromethyl group but also by the position to which the fluorines or trifluoromethyl group bonded. The results reveal that fluorines or trifluoromethyl group can increase oxidation potentials and reduce the energy level of HOMO, as observed in previous report. In addition, the 4FPZ-based complex shows more positive oxidation potential than the corresponding acac-based complex (i.e., E_{onset} = 1.01 V for **15** and E_{onset} = 0.81 V for **6**), clearly indicating that the triazolpyridine has the stronger ability to reduce the energy level of HOMO than acac.

2.5. Electroluminescence Performance

2.5.1. Monochrome OLEDs

Considering that these iridium(III) phosphors possessing highly efficient emission from greenish–yellow to yellow and very broad emission (FWHM up to 103 nm), the complexes have been used for fabrication of OLEDs. To evaluate the EL performances, the monochrome OLEDs using iridium(III) complexes **9**, **13**, **15**, **17**, and **18** as the emitters were fabricated with the structures of indium tin oxide (ITO)/1,4,5,8,9,11-hexaazatriphenylene-hexacarbonitrile (HAT-CN) (2 nm)/di-[4-(*N*,*N*-ditolylamino)-phenyl]cyclohexane (TAPC) (35 nm)/1,3-di(9*H*-carbazol-9-yl) benzene (mCP): *x*% Ir (10 nm)/1,3,5-tris(1-phenyl-1*H*-benzo[*d*] imidazol-2-yl)benzene (TPBi): *y*% Ir (10 nm)/TmPyPb (30 nm)/Liq (1 nm)/Al (150 nm). As shown in Figure S13a (Supporting Information), the ITO acts as anode, HAT-CN acts as hole injection layer (HIL), TAPC acts as hole-transporting layer (HTL), both mCP and TPBi layers doped with iridium(III) complexes act as emissive layer for the purpose of balanced carrier transportation in this layer, 1,3,5-tri(*m*-pyrid-3-yl-phenyl)benzene (TmPyPb) acts as electron-transporting layer (ETL), a 1 nm 8-hydroxyquinolinolato lithium (Liq) layer and a 150 nm aluminium act as cathode layer. The energy diagram of the monochrome devices and the molecular structures of the materials used are shown in Figure S14 and Scheme S4 (Supporting Information), respectively. To optimize the device efficiency, concentration dependence experiments were carried out for iridium(III) complex **13**. The optimized iridium(III) complexes with 8 wt% doping concentration in mCP and 15 wt% doping concentration in TPBi were used as the emitting layers (Table S7, Supporting Information). It can be seen in energy level diagram of OLEDs (Figure S14, Supporting Information) that the HOMO/LUMO levels of the iridium(III) complexes are all within those of the host materials mCP and TPBi. So, good carrier trapping is expected in these devices, which is the dominant EL mechanism. Furthermore, holes and electrons will be well confined within the doped light-emitting layer owing to the large energy gap (0.5 eV) between the HOMO of TPBi and the HOMO of TmPyPb.

The electroluminescence spectrum, current efficiency (η_c) versus luminance (L), power efficiency (η_p) versus luminance (L), and external quantum efficiency versus current density (J) characteristics of devices are shown in **Figure 3**. The L–V–J curves could be found in Figure S15a (Supporting Information). All OLEDs emit yellow or greenish–yellow light with the EL emission peaks at 564, 559, 550, 555, and 545 nm for iridium(III) complexes **9**, **13**, **15**, **17**, and **18**, respectively. As shown in Figure 3d, the EL spectra of all OLEDs exhibit dominant emission bands corresponding to the iridium(III) complex without any other residual emission band originating from host and/or adjacent layers, suggesting that excitons generated in emissive layer mainly deactivate by phosphorescence emission of iridium(III) complex. As shown in Figure S15b (Supporting Information) and **Table 2**, the CIE color coordinates of all OLEDs are in yellow or greenish–yellow region of the CIE chromaticity diagram. In addition, the close resemblance between the PL and EL spectra (Figure S16, Supporting Information) suggests that the EL emission of all monochrome OLEDs originates from the unimolecular triplet excited states of the phosphors instead of excimer emission. It is highlighted that all yellow or greenish–yellow-emitting OLEDs exhibit very broad emission band with FWHMs in the range of 94–102 nm, and, more importantly, these high values in FWHMs do not rely on the presence of excimer emission. As previously discussed, the use of excimer emission can effectively broaden the EL spectrum of yellow-emitting OLEDs, however, the EL spectra and the corresponding CIE are greatly influenced by the dopant concentration. To the best of our knowledge, the FWHMs of our novel iridium(III) complex-based OLEDs are among the highest values of yellow or greenish-yellow-emitting OLEDs without excimer emission reported in the literature, as summarized in Table S8 (Supporting Information). Especially, the FWHM of OLED based on complex **9** is up to 102 nm, which

© 2015 WILEY-VCH Verlag GmbH & Co. KGaA, Weinheim

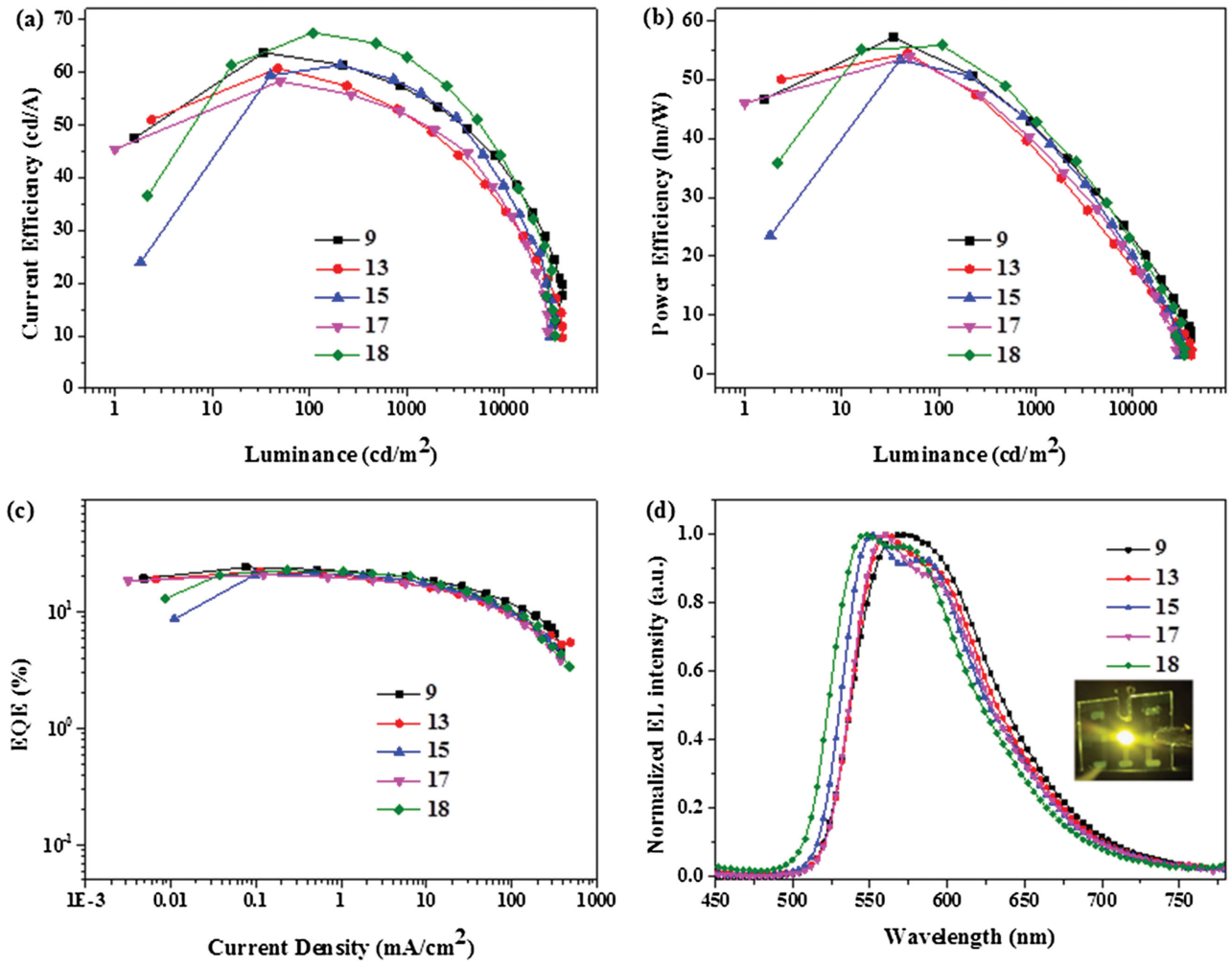

Figure 3. a) The η_c–L curves, b) η_p–L curves, c) EQE–J curves, and d) EL spectra of the yellow and greenish–yellow emitting devices based on iridium(III) complexes **9**, **13**, **15**, **17**, and **18**. Inset: EL photograph of device based on complex **13**.

is competitive with the reported yellow OLEDs by utilizing excimer emission.[43]

The monochrome OLEDs based on iridium(III) complexes **9**, **13**, **15**, **17**, and **18** also exhibit encouraging EL performances, as summarized in Table 2. All devices exhibit low turn-on voltages ($V_{turn\text{-}on}$) around 3.0 V (defined as bias at a luminance of 1 cd m^{-2}). The maximum luminance of the OLEDs is in the range of 28 204–39 872 cd m^{-2}. The maximum η_c, η_p, and EQE of OLEDs based on iridium(III) complexes **9**, **13**, **15**, **17**, and **18** are in the range of 58.3–67.5 cd A^{-1}, 53.3–57.2 lm W^{-1}, and 20.8%–24.1%, respectively. Especially, the maximum EQE of OLED based on iridium(III) complex **9** is up to 24.1%, which is the highest value among the reported yellow or greenish–yellow OLEDs.[47]

Table 2. Electroluminescence data for the devices.

Complex	λ_{EL} [nm]	CIE[a] (x, y)	V_{ON}[b] [V]	L_{max} [cd m^{-2}]	η_{cmax} [cd A^{-1}]	η_{pmax} [lm W^{-1}]	EQE_{max} [%]	FWHM [nm]
9	564	(0.52, 0.47)	3.0	40 011	63.8	57.2	24.1	102
13	559	(0.51, 0.47)	3.0	39 872	60.7	54.5	22.2	94
15	550	(0.50, 0.49)	3.0	31 613	61.4	53.3	21.4	99
17	555	(0.51, 0.48)	3.0	28 204	58.3	53.9	20.8	96
18	545	(0.47, 0.50)	3.1	33 571	67.5	55.8	22.7	100

[a]Current density is 100 mA cm^{-2}; [b]Luminance is 1 cd m^{-2}.

© 2015 WILEY-VCH Verlag GmbH & Co. KGaA, Weinheim

It has been reported that the exciplex can be formed in donor–acceptor cohost doping system (e.g., mCP:TPBi), which enables efficient singlet and triplet energy transfer from the host exciplex to the phosphorescent dopant.[35,42,67–69] So, the generation of exciplex in mCP:TPBi is beneficial for increasing EQE of yellow OLEDs. However, different from exciplex in mCP:TPBi cohost doping system (≈20 nm),[67–69] the mCP and TPBi in our yellow OLEDs were double separated layers, in which the exciplex could be only formed in the mCP:TPBi interface area (about several nm). The contribution of exciplex in mCP:TPBi interface to high EQE is not significant, and the carrier trapping effect of lepidine-based iridium(III) complexes mainly contributes to high EQE of yellow OLEDs. In addition, the overlap between the PL spectrum of the exciplex and the UV–vis absorption spectrum of iridium(III) complexes is the basic requirement for the energy transfer from the exciplex to iridium(III) complexes.[68,69] For acquiring high energy-transfer efficiency, the spectra overlap should be large. However, the overlap between the PL spectrum of the exciplex of mCP:TPBi[67] and the absorption of the lepidine-based iridium(III) complexes (as shown in Figure 2a,c) is not large enough for high energy-transfer efficiency, further indicating small contribution of exciplex to high EQE in our OLEDs.

2.5.2. White OLEDs

Considering that these iridium(III) complexes exhibit very broad emission band covering the greenish–yellow to red region in EL spectra, which is very significant for high-quality complementary-color WOLEDs (such as CRI), the WOLED containing the blue emission layer and the yellow emission layer was designed and fabricated in this work. We chose iridium(III) complex **18** as the yellow phosphorescent emitter and BmPAC (chemical structure shown in Scheme S4, Supporting Information) as blue fluorescent emitter previously reported by us.[70] So, the fluorescent-phosphorescent hybrid WOLED with symmetrical cascade emissive layer structure (Figure S13b, Supporting Information) of ITO/HAT-CN (2.5 nm)/*N*,*N*′-bis(naphthalen-1-yl)-*N*,*N*′-bis(phenyl)benzidine (NPB) (20 nm)/TCTA (10 nm)/mCP: 15% Ir**18** (5 nm)/mCP (3 nm)/9,10-di(naphthalen-2-yl)anthracene (ADN): 3% BmPAC (4 nm)/mCP (3 nm)/mCP: 15% Ir**18** (5 nm)/TPBi (30 nm)/Liq (1 nm)/Al (150 nm) were fabricated. In the WOLED, the HAT-CN, NPB and tris(4-(9*H*-carbazol-9-yl)phenyl)amine (TCTA), TPBi and Liq/Al act as HIL, HTL, ETL and cathode, respectively. Herein, we used mCP as the host material for the highly efficient energy transfer from mCP to complex **18** owing to its higher triplet energy level (2.90 eV) than that of complex **18**

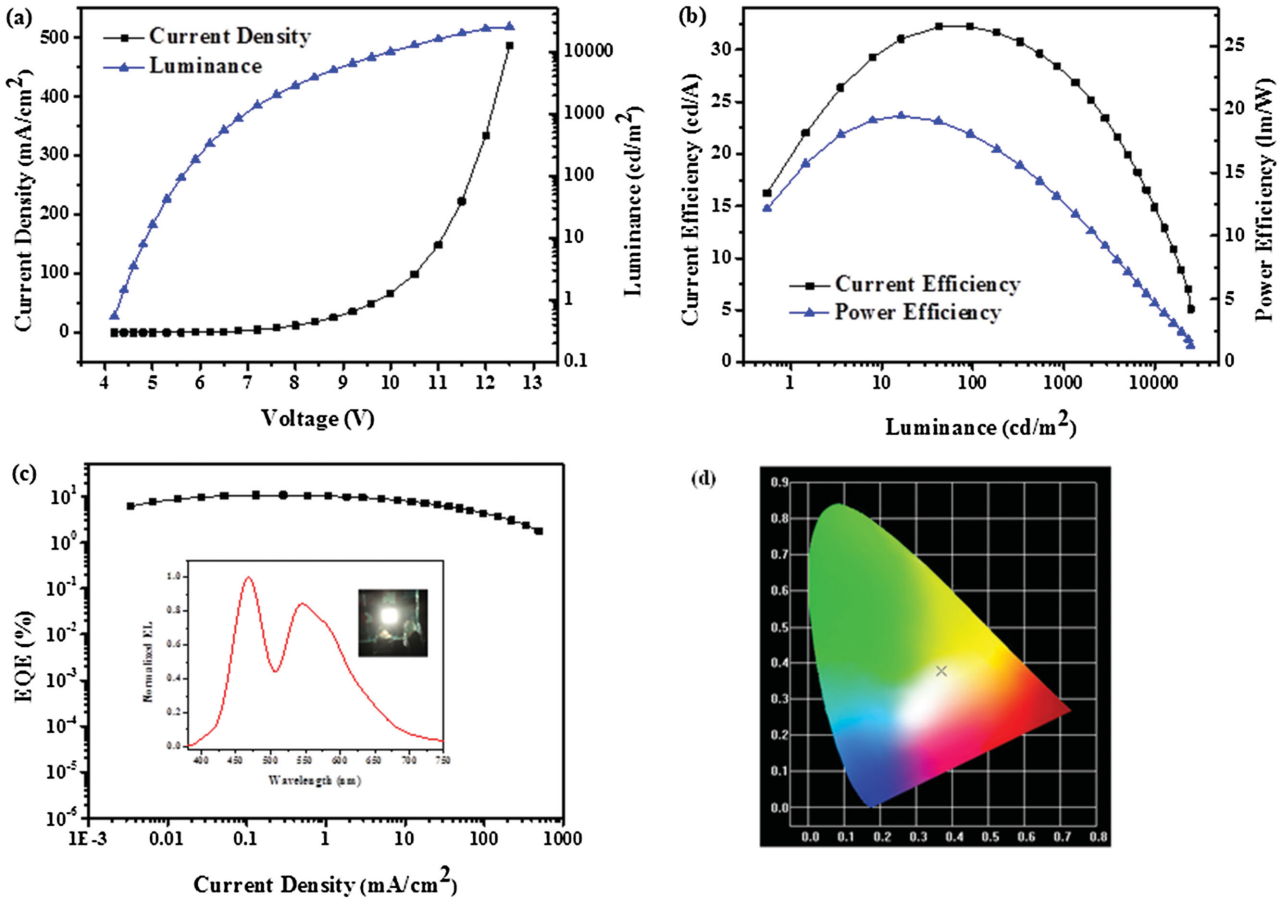

Figure 4. a) The *J*–*V*–*L* curves, b) η_c–*L*–η_p curves, c) EQE–*J* curves, d) and 1931 CIE coordinates of the white device. Inset: EL spectrum and corresponding photograph of white device.

© 2015 WILEY-VCH Verlag GmbH & Co. KGaA, Weinheim

(2.34 eV) and used ADN as the host for fluorescent blue emitter BmPAC. The energy diagram of the WOLED is shown in Figure S17 (Supporting Information). The η_c, η_p versus L and EQE versus J of the WOLED can be found in **Figure 4**, and the inset shows its EL spectrum and photograph at 2000 cd m^{-2}. As shown in Figure 4c, it can be seen that the EL spectrum of WOLED exhibits double emission peaks located at 467 and 545 nm, respectively, covering nearly all visible light region with the CRI as high as 78, which is very close to the critical value (80) required for the practical solid-state lighting applications. It is believed that the CRI of this WOLED can be further improved (over 80) by using a deep-blue emitter. As far as we known, there are few reports of such a high CRI, especially for the devices with wide spectra covering the white region based on two colors without excimer emission, which usually exhibit the CRI in the range of 50–65, as summarized in Table S9 (Supporting Information). Such a high CRI of the two complementary colors-based WOLED was attributed to the well-matched emission spectra, especially the very broad FWHM (up to 100 nm) of the greenish–yellow emitter **18**. As shown in Figure 4d and Table S10 (Supporting Information), the CIE color coordinates of WOLED is (0.37, 0.38) at 2000 cdm^{-2}, corresponding to the white-light region in CIE chromaticity diagram. Moreover, the WOLED display low turn-on voltages of 3.5 V, high luminance of 22 019 cd m^{-2}, the maximum current efficiency of 32.2 cd A^{-1}, the maximum power efficiency of 19.5 lm W^{-1}, and the maximum external quantum efficiency of 10.7%, respectively. We believe that the efficiencies of the WOLED fabricated could be further improved by optimizing the doping ratio of iridium(III) complexes, choosing more suitable host materials or using a blue phosphorescent emitter without compromising the CRI of the WOLEDs.

3. Conclusion

In summary, we developed a facile synthetic route, that is, using dichloromethane as solvent and anhydrous potassium carbonate as deacid reagent at room temperature to prepare both β-diketonates-based and triazolpyridine-based neutral iridium(III) complexes in excellent yields, which is a promising method for the future large-scale preparation of phosphorescent materials. Based on the facile synthetic method, two series of new fluorine atoms and (or) trifluoromethyl group modified lepidine-based phosphorescent iridium(III) complexes have been prepared with pentane-2,4-dione or triazolpyridine as ancillary ligands, respectively. And the effects of fluorine atoms and (or) trifluoromethyl group on tuning optical properties of two series of complexes have been examined in detail. All triazolpyridine-based complexes display blueshifted dual-peak emission compared to pentane-2,4-dione-based complexes with a broad single-peak emission. The complexes show emission with FWHM up to 103 nm, and their emission colors vary from greenish–yellow, yellow, orange-yellow to orange. Among them, the iridium(III) complex **18** exhibits the quantum yields up to 0.92, which is the highest one among the reported neutral yellow iridium(III) complexes. Highly efficient monochrome OLEDs and WOLEDs have been fabricated. The FWHMs of the monochrome OLEDs in the range of 94–102 nm, which are among the highest values of the reported yellow or greenish–yellow OLEDs without excimer emission. The maximum EQE of monochrome OLEDs based on iridium(III) complexes **9**, **13**, **15**, **17**, and **18** are in the range of 20.8%–24.1%, respectively. Especially, the maximum EQE of OLEDs based on iridium(III) complex **9** is up to 24.1%, which is the highest value among the reported yellow or greenish–yellow devices. The CRI of blue and complementary yellow-based WOLED is as high as 78. These preliminary results obtained indicated that this family of highly emissive greenish–yellow and yellow neutral iridium(III) complexes based on fluorine modified cyclometalated lepidine-based ligands are the promising candidates for the WOLEDs, which is of great significance for the development of solid-state lighting techniques.

4. Experimental Section

General Experimental Information: All operations were performed under an inert nitrogen atmosphere using standard Schlenk unless otherwise stated. All solvents were used after distillation and stored over activated molecular sieves (5 Å). All reagents and chemicals were purchased from commercial sources and used without further purification. Aniline, ethyl 3-oxobutanoate, concentrated sulfuric acid, phosphorus oxychloride, tetrakis(triphenylphosphine)palladium(0), iridium(III) trichloride hydrate, pentane-2,4-dione (Hacac), and iridium(III) tris(acetylacetonate) ($Ir(acac)_3$) were obtained from Acros. Deuterated solvents from Cambridge Isotope Laboratories were used. The NMR spectra were recorded with a Bruker spectrometer at 600 or 400 MHz (600 or 400 MHz for ^1H, 150 or 100 MHz for ^{13}C) at ambient temperature. Chemical shifts are given in ppm and are referenced against external Me_4Si (^1H, ^{13}C). Mass spectra were obtained on SHIMADZU matrix-assisted laser desorption/ionization time-of-flight mass pectrometer (MALDI-TOF-MASS). Elemental analyses were carried out with a VarioEL III O-Element Analyzer system. The UV–vis spectra were recorded on a Shimadzu UV-2550 spectrometer. Steady-state emission experiments at room temperature or 77 K were measured on an Edinburgh LFS-920 spectrometer. Excited-state lifetime studies were performed with an Edinburgh LFS-920 spectrometer with a hydrogen-filled excitation source. The data were analyzed by iterative convolution of the luminescence decay profile with the instrument response function using a software package provided by Edinburgh Instruments. The absolute quantum yields of the complexes were determined through an absolute method by employing an integrating sphere. The solution was degassed by three freeze–pump–thaw cycles. Cyclic voltammetry measurements were carried out in acetonitrile (5×10^{-4} M) with a three-electrode cell configuration consisting of platinum working and counter electrodes and an $Ag/AgNO_3$ (0.01 M in CH_3CN) reference electrode at room temperature. Tetra-*n*-butylammonium hexafluorophosphate (0.1 M in CH_2Cl_2) was used as the supporting electrolyte. The redox potentials were recorded at a scan rate of 100 mV s^{-1} and are reported with reference to the ferrocene/ferrocenium (Fc/Fc^+) redox couple. The ancillary H*N*^*N* ligand 2-(3-(4-fluorophenyl)-1*H*-1,2,4-triazol-5-yl)pyridine (H4FPZ) was synthesized according to the literature procedures.[71]

Synthesis of the Cyclometalated HC^N Ligands: The synthetic routes (Scheme S1, Supporting Information) of the cyclometalated HC^*N* ligands (HMePQ, HMePQ-4F, HMePQ-24F, HMePQ-234F, HMePQ-35F, HMePQ-345F, HMePQ-2345F, HMePQ-$3CF_3$, and HMePQ-$3CF_3$-4F) were synthesized by highly efficient Suzuki coupling reactions. 2-chloro-4-methylquinoline was synthesized by three-step reactions in overall yield of 74% and can be found in the Supporting Information. Herein, a detailed description was provided only for HMePQ-234F.

4-Methyl-2-(2,3,4-trifluorophenyl)quinoline (HMePQ-234F): $Pd(PPh_3)_4$ (320 mg, 0.28 mmol) was added to a mixture of 2-chloro-4-methylquinoline

© 2015 WILEY-VCH Verlag GmbH & Co. KGaA, Weinheim

(c) (1.50 g, 8.45 mmol), 2,3,4-trifluorophenylboronic acid (1.03 g, 8.45 mmol), toluene (40 mL), methanol (10 mL), and 2.0 M potassium carbonate aqueous solution (20 mL) under vigorous stirring. The mixture was stirred at 80 °C for 24 h under N_2 atmosphere. After being cooled to room temperature, and extracted with dichloromethane, then washed with water, and dried over anhydrous Na_2CO_3, The solvent was removed under reduced pressure. The crude product was purified by column chromatography using a 80:1 mixture of petroleum ether and ethyl acetate as the eluent to give white crystalline powder (84% Yiled). ^{1}H NMR (600 MHz, $CDCl_3$, δ): 8.15 (d, J = 8.4 Hz, 1H), 8.01 (d, J = 8.4 Hz, 1H), 7.88–7.83 (m, 1H), 7.74 (ddd, J = 1.2 Hz, J = 6.6 Hz, J = 7.8 Hz, 1H), 7.66 (d, J = 2.4 Hz, 1H), 7.59 (ddd, J = 1.2 Hz, J = 7.2 Hz, J = 8.4 Hz, 1H), 7.14–7.1 (m, 1H), 2.76 (s, 3H); ^{13}C{^{1}H} NMR (100 MHz, $CDCl_3$, δ): 151.9 (ddd, J = 2.9 Hz, J = 2.3 Hz, J = 1.3 Hz), 151.7 (ddd, J = 250.7 Hz, J = 10.1 Hz, J = 3 Hz), 150.1 (ddd, J = 252.1 Hz, J = 10.8 Hz, J = 3.2 Hz), 148.2, 145.1, 140.3 (ddd, J = 249.1 Hz, J = 16 Hz, J = 15.3 Hz), 130.4, 129.7, 127.5, 126.9, 125.8 (ddd, J = 9.5 Hz, J = 3.8 Hz, J = 1.2 Hz), 125.1 (ddd, J = 7.8 Hz, J = 4.2 Hz, J = 3.5 Hz), 123.8, 122.6 (d, J = 7.8 Hz), 112.6 (dd, J = 17.3 Hz, J = 3.9 Hz), 19.1; ^{19}F{^{1}H} NMR (376 MHz, $CDCl_3$, δ): –133.2 (dd, J = 8.7 Hz, J = 20.7 Hz), –138.2 (dd, J = 8.7 Hz, J = 21.1 Hz), –160.3 (t, J = 20.7 Hz); Anal. calcd for $C_{16}H_{10}F_3N$: C 70.33, H 3.69, N 5.13; found: C 70.40, H 3.72, N 5.10.

Characterization data for HMePQ, HMePQ-4F, HMePQ-24F, HMePQ-35F, HMePQ-345F, HMePQ-2345F, HMePQ-3CF_3, and HMePQ-3CF_3-4F can be found in the Supporting Information.

Synthesis of Iridium(III) Complexes: The general procedures for each class of iridium(III) complexes are provided below.

General Procedure for the Synthesis of Ir(C^N)$_2$(acac) **1**–**9** (Scheme S2, Supporting Information): Cyclometalated iridium(III) μ-chlorobridged dimers of a general formula $(C^{\wedge}N)_2Ir(\mu\text{-}Cl)_2Ir(C^{\wedge}N)_2$ were synthesized according to the Nonoyama route,[63] by refluxing $IrCl_3{\cdot}3H_2O$ with 2.2 equiv of corresponding cyclometalated HC^N ligand in a 3:1 mixture of 2-ethoxyethanol and water. To the mixture of chlorobridged dimer (0.2 mmol) and anhydrous potassium carbonate(K_2CO_3) powder (2 mmol) were added dichloromethane (30 mL) and pentane-2,4-dione (0.5 mmol), and then the slurry was stirred at room temperature (≈25 °C) for 24 h without any inert gas protection. After the reaction was finished, the dichloromethane solution containing $Ir(C^{\wedge}N)_2(acac)$ was filtered to remove insoluble salts. The solvent was removed under reduced pressure. The crude products were purified by column chromatography using a 10:1 mixture of petroleum ether and CH_2Cl_2 as the eluent to give the target complexes, finally the complexes were recrystallized from CH_2Cl_2/hexane to remove trace soluble impurities.

Ir(MePQ-345F)$_2$(acac) **(6)**: Orange powder (90% yield). ^{1}H NMR (600 MHz, $CDCl_3$, δ): 8.23 (d, J = 8.4 Hz, 2H), 7.93 (dd, J = 1.2 Hz, J = 8.4 Hz, 2H), 7.75 (s, 2H), 7.58 (ddd, J = 0.6 Hz, J = 6.6 Hz, J = 10.8 Hz, 2H), 7.51 (ddd, J = 1.2 Hz, J = 6.6 Hz, J = 7.8 Hz, 2H), 7.44 (ddd, J = 1.2 Hz, J = 6.6 Hz, J = 8.4 Hz, 2H), 4.55 (s, 1H), 2.91 (s, 6H), 1.47 (s, 6H); ^{13}C{^{1}H} NMR (150 MHz, $CDCl_3$, δ): 185.2, 167.5 (d, J = 2.3 Hz), 157.8 (ddd, J = 2.4 Hz, J = 7.7 Hz, J = 237.9 Hz), 149.4, 147.8 (ddd, J = 3.3 Hz, J = 12 Hz, J = 238.8 Hz), 146.7, 144.1 (ddd, J = 4.1 Hz, J = 7.2 Hz, J = 16.1 Hz), 139.8 (ddd, J = 15.3 Hz, J = 20.1 Hz, J = 255.2 Hz), 130.2, 126.8, 126.7, 126.3, 126.1 (d, J = 32.6 Hz), 124.0, 117.8, 110.0 (dd, J = 3 Hz, J = 17.7 Hz), 100.1, 28.1, 19.4; ^{19}F{^{1}H} NMR (376 MHz, $CDCl_3$, δ): –128.4 (dd, J = 4.1 Hz, J = 24.1 Hz), –144.8 (dd, J = 4.1 Hz, J = 19.9 Hz), –159.6 (dd, J = 19.6 Hz, J = 24.1 Hz); MALDI-TOF-MS (m/z): calcd for $C_{37}H_{25}F_6IrN_2O_2$, 836.14; found, 836.02.

Characterization data for complex **1**, **2**, **3**, **4**, **5**, **7**, **8**, and **9** can be found in the Supporting Information.

General Procedure for the Synthesis of Ir(C^N)$_2$(4FPZ) **10**–**18** (Scheme S2, Supporting Information): To the mixture of chlorobridged dimer $(C^{\wedge}N)_2Ir(\mu\text{-}Cl)_2Ir(C^{\wedge}N)_2$ (0.2 mmol) and anhydrous potassium carbonate (K_2CO_3) powder (2 mmol) were added dichloromethane (30 mL) and H4FPZ (0.5 mmol), and then the slurry was stirred at room temperature (≈25 °C) for 24 h without any inert gas protection. After the reaction was finished, the dichloromethane solution containing $Ir(C^{\wedge}N)_2$(4FPZ) was filtered to remove insoluble salts. The solvent was removed under reduced pressure. The crude product was purified by column chromatography using CH_2Cl_2 as the eluent to give target complexes.

Ir(MePQ-3CF_3-4F)$_2$(4FPZ) (**18**): Yellow powder (85% yield). ^{1}H NMR (600 MHz, DMSO-d_6, δ): 8.67 (d, J = 7.2 Hz, 1H), 8.66 (s, 1H), 8.62 (s, 1H), 8.56 (d, J = 7.8 Hz, 1H), 7.98 (t, J = 8.4 Hz, 2H), 7.93 (d, J = 5.4 Hz, 1H), 7.88 (dt, J = 1.2 Hz, J = 7.8 Hz, 1H), 7.84–7.81 (m, 3H), 7.72 (d, J = 7.8 Hz, 1H), 7.46 (t, J = 7.2 Hz, 1H), 7.43 (t, J = 7.8 Hz, 1H), 7.40 (ddd, J = 1.2 Hz, J = 6 Hz, J = 7.2 Hz, 1H), 7.34 (d, J = 9 Hz, 1H), 7.18–7.14 (m, 2H), 7.07 (ddd, J = 1.2 Hz, J = 7.8 Hz, J = 9 Hz, 1H), 7.04 (ddd, J = 1.2 Hz, J = 7.2 Hz, J = 8.4 Hz, 1H), 6.43 (d, J = 11.4 Hz, 1H), 6.22 (d, J = 11.4 Hz, 1H), 2.9 (s, 3H), 2.85 (s, 3H); ^{19}F{^{1}H} NMR (376 MHz, DMSO-d_6, δ): –58.8 (d, J = 12 Hz), –59.0 (d, J = 12 Hz), –114.3 (s), –115.0 (q, J = 12 Hz), –115.8 (q, J = 12 Hz); MALDI-TOF-MS (m/z): calcd for $C_{47}H_{28}F_9IrN_6$, 1040.19; found, 1040.45.

Characterization data for complex **10**, **11**, **12**, **13**, **14**, **15**, **16**, and **17** can be found in the Supporting Information.

EL Device Fabrication: The devices were fabricated on the prepatterned ITO glass substrate with sheet resistance of 10 Ω sq^{-1} by vacuum deposition. ITO substrates as the anode were scrubbed and sonicated consecutively with detergent water, deionized water, and acetone, dried in drying cabinet, and then exposed to a UV-ozone environment for 10 min. After these processes, the substrates were transferred into a vacuum chamber for sequential deposition of all organic functional layers by thermal evaporation below a vacuum of 5×10^{-4} Pa. The deposition rates for organic materials, 8-hydroxyquinolinolato lithium (Liq), and aluminium, were ≈1, 0.1, and 3 Å s^{-1}, respectively. The thickness of the films was controlled by a quartz thickness monitor. The active layer of devices is 3×3 mm^2. The current–voltage–forward luminance characteristics, color rendering indexes, CIE coordinates were measured with a PR655 Spectrascan spectrometer and a Keithley 2400 programmable voltage current source. All the samples were measured directly after fabrication without encapsulation in ambient atmosphere at room temperature.

X-Ray Crystallography Analysis: The X-ray diffraction data were collected on a Bruker Smart CCD Apex DUO diffractometer with graphite monochromated M_o K_α radiation (λ = 0.71073 Å) using the ω–2θ scan mode. The data were corrected for Lorenz and polarization effects. The structure was solved by direct methods and refined on F^2 by full-matrix least-squares methods using SHELXTL-2000. All calculations and molecular graphics were carried out on a computer using the SHELX-2000 program package and Mercury. Crystallographic data for the structural analyses have been deposited with the Cambridge Crystallographic Data Center (CCDC). CCDC reference numbers for **1**, **2**, **4**, **6**, **7**, **9**, and **15** are 1 421 363, 1 421 364, 1 421 366, 1 421 368, 1 421 369, 1 421 365, and 1 421 367, respectively. Copies of this information can be obtained free of charge from The Director, CCDC, 12 Union Road, Cambridge, CB2 1EZ, UK (Fax: +441223336033; E-mail: deposit@ccdc.cam.ac.uk, or www: http://www.ccdc.cam.ac.uk).

Supporting Information

Supporting Information is available from the Wiley Online Library or from the author.

Acknowledgements

The authors thank Program for New Century Excellent Talents in University of Ministry of Education of China (NCET-13-0927), National Natural Scientific Foundation of China (Grant Nos. 61205179, 61274018 and 21471111), Natural Science Foundation of Jiangsu Province of China (Grant Nos. BK20130038, BM2012010 and BM2012010), Scientific and Technological Innovation Teams of Colleges and Universities in Jiangsu Province (TJ215006), Jiangsu National Synergetic Innovation Center for Advanced Materials (SICAM), Shanxi Provincial Key Innovative Research Team in Science and Technology (Grant No. 2012041011), Synergetic

© 2015 WILEY-VCH Verlag GmbH & Co. KGaA, Weinheim

Innovation Center for Organic Electronics and Information Displays, Specialized Research Fund for the Doctoral Program of Higher Education (20113223110005), and Priority Academic Program Development of Jiangsu Higher Education Institutions (Grant No. YX03001) for financial support.

Received: September 9, 2015
Revised: October 24, 2015
Published online: December 21, 2015

[1] S. Lamansky, P. Djurovich, D. Murphy, F. Abdel-Razzaq, H. E. Lee, C. Adachi, P. E. Burrows, S. R. Forrest, M. E. Thompson, *J. Am. Chem. Soc.* **2001**, *123*, 4304.
[2] J. Li, P. I. Djurovich, B. D. Alleyne, M. Yousufuddin, N. N. Ho, J. C. Thomas, J. C. Peters, R. Bau, M. E. Thompson, *Inorg. Chem.* **2005**, *44*, 1713.
[3] Y. Chi, P. T. Chou, *Chem. Soc. Rev.* **2010**, *39*, 638.
[4] M. C. Tang, D. P. K. Tsang, V. W. W. Yam, *Angew. Chem. Int. Ed.* **2013**, *52*, 446.
[5] G. Cheng, K. T. Chan, W. P. To, C. M. Che, *Adv. Mater.* **2014**, *26*, 2540.
[6] X. Wang, Y. L. Chang, J. S. Lu, T. Zhang, Z. H. Lu, S. Wang, *Adv. Funct. Mater.* **2014**, *24*, 1911.
[7] D. B. Xia, B. Wang, B. Chen, S. M. Wang, B. H. Zhang, J. Q. Ding, L. X. Wang, X. B. Jing, F. S. Wang, *Angew. Chem. Int. Ed.* **2014**, *53*, 1048.
[8] H. Li, H. M. Zhan, L. X. Wang, *Inorg. Chem.* **2014**, *53*, 810.
[9] X. B. Xu, G. J. Zhou, W. Y. Wong, *Chem. Commun.* **2014**, *50*, 2473.
[10] W. W. Tian, W. Jiang, Y. M. Sun, *J. Mater. Chem. C* **2014**, *2*, 1104.
[11] R. J. Wang, D. Liu, J. Y. Li, *Adv. Mater.* **2011**, *23*, 2823.
[12] C. L. Yang, D. G. Ma, J. G. Qin, *Adv. Funct. Mater.* **2007**, *17*, 651.
[13] S. Haneder, E. D. Como, J. Feldmann, *Adv. Mater.* **2008**, *20*, 3325.
[14] J. Q. Ding, B. Wang, L. X. Wang, *Angew. Chem. Int. Ed.* **2009**, *48*, 6664.
[15] W. Y. Wong, C. L. Ho, Z. Y. Lin, *Angew. Chem. Int. Ed.* **2006**, *45*, 7800.
[16] Y. Sun, N. C. Giebink, H. Kanno, B. Ma, M. E. Thompson, S. R. Forrest, *Nature* **2006**, *440*, 908.
[17] V. N. Kozhevnikov, Y. H. Zheng, A. P. Monkman, *Chem. Mater.* **2013**, *25*, 2352.
[18] B. H. Zhang, G. P. Tan, C. S. Lam, B. Yao, C. L. Ho, L. H. Liu, Z. Y. Xie, W. Y. Wong, J. Q. Ding, L. Wang, *Adv. Mater.* **2012**, *24*, 1873.
[19] S. Reineke, F. Lindner, G. Schwartz, N. Seidler, K. Walzer, B. Luessem, K. Leo, *Nature* **2009**, *459*, 234.
[20] G. Schwartz, S. Reineke, T. C. Rosenow, *Adv. Funct. Mater.* **2009**, *19*, 1319.
[21] Q. Zhao, S. J. Liu, M. Shi, C. M. Wang, M. X. Yu, L. Li, F. Y. Li, T. Yi, C. H. Huang, *Inorg. Chem.* **2006**, *45*, 6152.
[22] C. Shi, H. B. Sun, X. Tang, W. Lv, H. Yan, Q. Zhao, J. X. Wang, W. Huang, *Angew. Chem. Int. Ed.* **2013**, *52*, 13434.
[23] C. Shi, H. B. Sun, Q. B. Jiang, Q. Zhao, J. X. Wang, W. Huang, H. Yan, *Chem. Commun.* **2013**, *49*, 4746.
[24] G. J. Zhou, C. L. Ho, W. Y. Wong, Q. Wang, D. G. Ma, L. X. Wang, Z. Y. Lin, T. B. Marder, A. Beeby, *Adv. Funct. Mater.* **2008**, *18*, 499.
[25] X. Mou, Y. Q. Wu, S. J. Liu, M. Shi, X. M. Liu, C. M. Wang, S. Sun, Q. Zhao, X. H. Zhou, W. Huang, *J. Mater. Chem.* **2011**, *21*, 13951.
[26] Y. Wang, S. M. Wang, S. Y. Shao, J. Q. Ding, L. X. Wang, X. B. Jing, F. S. Wang, *Dalton Trans.* **2015**, *44*, 1052.
[27] Y. Wang, S. M. Wang, N. Zhao, B. X. Gao, S. Y. Shao, J. Q. Ding, L. X. Wang, X. B. Jing, F. S. Wang, *Polym. Chem.* **2015**, *6*, 1180.
[28] Z. Q. Chen, Z. Q. Bian, C. H. Huang, *Adv. Mater.* **2010**, *22*, 1534.
[29] W. C. H. Choy, W. K. Chan, Y. P. Yuan, *Adv. Mater.* **2014**, *26*, 2368.
[30] H. B. Sun, S. J. Liu, W. P. Lin, K. Y. Zhang, W. Lv, X. Huang, F. W. Huo, H. R. Yang, G. Jenkins, Q. Zhao, W. Huang, *Nat. Commun.* **2014**, *5*, 3601.
[31] J. M. Fernandez-Hernandez, J. I. Beltran, V. Lemaur, M. D. Galvez-Lopez, C. H. Chien, F. Polo, E. Orselli, R. Fröhlich, J. Cornil, L. De Cola, *Inorg. Chem.* **2013**, *52*, 1812.
[32] C. Ulbricht, B. Beyer, C. Friebe, A. Winter, U. S. Schubert, *Adv. Mater.* **2009**, *21*, 4418.
[33] Y. L. Chang, B. A. Kamino, Z. B. Wang, M. G. Helander, Y. L. Rao, L. Chai, S. N. Wang, T. P. Bender, Z. H. Lu, *Adv. Funct. Mater.* **2013**, *23*, 3204.
[34] Z. S. Zhang, S. Z. Yue, Y. K. Wu, P. R. Yan, Q. Y. Wu, D. L. Qu, S. Y. Liu, Y. Zhao, *Optics Express* **2014**, *22*, 1815.
[35] S. L. Lai, S. L. Tao, M. Y. Chan, M. F. Lo, T. W. Ng, S. T. Lee, W. M. Zhao, C. S. Lee, *J. Mater. Chem.* **2011**, *21*, 4983.
[36] H. Kanno, R. Holmes, Y. Sun, S. K. Cohen, S. Forrest, *Adv. Mater.* **2006**, *18*, 339.
[37] X. F. Qi, M. Slootsky, S. Forrest, *Appl. Phys. Lett.* **2008**, *93*, 193306.
[38] T. W. Lee, T. Y. Noh, B. K. Choi, M. S. Kim, D. W. Shin, J. Kido, *Appl. Phys. Lett.* **2008**, *92*, 043301.
[39] B. D. Andrade, R. Holmes, S. Forrest, *Adv. Mater.* **2004**, *16*, 624.
[40] D. M. Kang, J. W. Kang, J. W. Park, S. O. Jung, S. H. Lee, H. D. Park, Y. H. Kim, S. C. Shin, J. J. Kim, S. K. Kwon, *Adv. Mater.* **2008**, *20*, 2003.
[41] S. Chen, G. Tan, W. Wong, H. Kwok, *Adv. Funct. Mater.* **2011**, *21*, 3785.
[42] S. L. Lai, S. L. Tao, M. Y. Chan, T. W. Ng, M. F. Lo, C. S. Lee, X. H. Zhang, S. T. Lee, *Org. Electron.* **2010**, *11*, 1511.
[43] M. Li, W. H. Chen, M. T. Lin, M. A. Omary, N. D. Shepherd, *Org. Electron.* **2009**, *10*, 863.
[44] I. R. Laskar, S. F. Hsu, T. M. Chen, *Polyhedron* **2005**, *24*, 881.
[45] J. Y. Li, R. J. Wang, R. X. Yang, W. Zhou, X. Wang, *J. Mater. Chem. C* **2013**, *1*, 4171.
[46] V. K. Rai, M. Nishiura, M. Takimoto, S. Zhao, Y. Liu, Z. M. Hou, *Inorg. Chem.* **2012**, *51*, 822.
[47] J. H. Jou, Y. X. Lin, S. H. Peng, C. J. Li, Y. M. Yang, C. L. Chin, J. J. Shyue, S. S. Sun, M. Lee, C. T. Chen, M. C. Liu, C. C. Chen, G. Y. Chen, J. H. Wu, C. H. Li, C. F. Sung, M. J. Lee, J. P. Hu, *Adv. Funct. Mater.* **2014**, *24*, 555.
[48] F. Dumur, M. Lepeltier, H. Z. Siboni, D. Gigmes, H. Aziz, *Adv. Optical Mater.* **2014**, *2*, 262.
[49] H. B. Wu, J. H. Zou, F. Liu, L. Wang, A. Mikhailovsky, G. C. Bazan, W. Yang, Y. Cao, *Adv. Mater.* **2008**, *20*, 696.
[50] H. B. Wu, G. J. Zhou, J. H. Zou, C. L. Ho, W. Y. Wong, W. Yang, J. B. Peng, Y. Cao, *Adv. Mater.* **2009**, *21*, 4181.
[51] S. H. Ye, T. Q. Hu, Z. Zhou, M. Yang, M. H. Quan, Q. B. Mei, B. C. Zhai, Z. H. Jia, W. Y. Lai, W. Huang, *Phys. Chem. Chem. Phys.* **2015**, *17*, 8860.
[52] K. R. J. Thomas, M. Velusamy, P. T. Chou, *Inorg. Chem.* **2005**, *44*, 5677.
[53] D. H. Kim, N. S. Cho, H. Y. Oh, J. H. Yang, W. S. Jeon, J. S. Park, M. C. Suh, J. H. Kwon, *Adv. Mater.* **2011**, *23*, 2721.
[54] K. H. Kim, S. H. Lee, C. K. Moon, S. Y. Kim, Y. S. Park, J. H. Lee, J. W. Lee, J. Huh, Y. M. You, J. J. Kim, *Nat. Commun.* **2014**, *5*, 4769.
[55] Q. Zhao, C. Y. Jiang, M. Shi, F. Y. Li, T. Yi, Y. Cao, C. H. Huang, *Organometallics* **2006**, *25*, 3631.
[56] M. S. Park, H. J. Park, O. Y. Kim, J. Y. Lee, *Org. Electron.* **2013**, *14*, 1504.
[57] Y. M. You, S. Y. Park, *J. Am. Chem. Soc.* **2005**, *127*, 12438.
[58] J. H. Jou, C. C. Chen, W. B. Wang, M. F. Hsu, C. J. Wang, C. T. Chen, M. F. Wu, H. Y. Chen, J. J. Shyue, C. L. Chin, *Proc. SPIE* **2008**, *7051*, 70510P.
[59] V. V. Grushin, N. Herron, D. D. LeCloux, W. J. Marshall, V. A. Petrov, Y. Wang, *Chem. Commun.* **2001**, *16*, 1494.
[60] Z. A. Bao, A. J. Lovinger, J. Brown, *J. Am. Chem. Soc.* **1998**, *120*, 207.

© 2015 WILEY-VCH Verlag GmbH & Co. KGaA, Weinheim

[61] C. H. Chang, C. L. Ho, Y. S. Chang, I. C. Lien, C. H. Lin, Y. W. Yang, J. L. Liao, Y. Chi, *J. Mater. Chem. C* **2013**, *1*, 2639.
[62] J. Sun, H. Wang, H. X. Xu, J. Li, Y. L. Wu, X. G. Du, B. S. Xu, *Mater. Chem. Phys.* **2015**, *162*, 392.
[63] K. Nonoyama, *Bull. Chem. Soc. Jpn.* **1974**, *47*, 467.
[64] R. J. Wang, D. Liu, H. C. Ren, T. Zhang, H. M. Yin, G. Y. Liu, J. Y. Li, *Adv. Mater.* **2011**, *23*, 2823.
[65] E. Orselli, G. S. Kottas, A. E. Konradsson, P. Coppo, R. Frohlich, L. D. Cola, A. V. Dijken, M. Buchel, H. Borner, *Inorg. Chem.* **2007**, *46*, 11082.
[66] F. O. Garces, K. A. King, R. J. Watts, *Inorg. Chem.* **1988**, *27*, 3464.
[67] T. Y. Zhang, B. Zhao, B. Chu, W. L. Li, Z. S. Su, L. J. Wang, J. B. Wang, F. M. Jin, X. W. Yan, Y. Gao, H. R. Wu, C. Y. Liu, T. Lin, F. H. Hou, *Org. Electron.* **2015**, *24*, 1.
[68] Y. S. Park, S. H. Lee, K. H. Kim, S. Y. Kim, J. H. Lee, J. J. Kim, *Adv. Funct. Mater.* **2013**, *23*, 4914.
[69] S. H. Lee, K. H. Kim, D. Limbach, Y. S. Park, J. J. Kim, *Adv. Funct. Mater.* **2013**, *23*, 4105.
[70] N. Wei, K. P. Guo, P. C. Zhou, J. N. Yu, B. Wei, J. H. Zhang, *Chin. Phys. B* **2014**, *23*, 77802.
[71] H. X. Xu, Y. Yue, L. T. Qu, Y. Y. Hao, H. Wang, L. Q. Chen, B. S. Xu, *Dyes Pigm.* **2013**, *99*, 67.

© 2015 WILEY-VCH Verlag GmbH & Co. KGaA, Weinheim